NANO · MICRO small
www.small-journal.com

Goat Milk Exosomes As Natural Nanoparticles for Detecting Inflammatory Processes By Optical Imaging

Ana Santos-Coquillat, María Isabel González, Agustín Clemente-Moragón, Mario González-Arjona, Virginia Albaladejo-García, Héctor Peinado, Javier Muñoz, Pilar Ximénez Embún, Borja Ibañez, Eduardo Oliver, Manuel Desco, and Beatriz Salinas**

Exosomes are cell-derived nanovesicles with a proven intercellular signaling role in inflammation processes and immune response. Due to their natural origin and liposome-like structure, these nanometer-scale vesicles have emerged as novel platforms for therapy and diagnosis. In this work, goat milk exosomes are isolated and fully characterized in terms of their physicochemical properties, proteomics, and biochemical profile in healthy mice, and used to detect inflammatory processes by optical imaging. For the in vitro and in vivo experiments, the exosomes are covalently labeled with the commercial fluorophores sulfo-Cyanine 5 and BODIPY-FL to create nanoprobes. In vitro studies using confocal imaging, flow cytometry, and colorimetric assays confirm the internalization of the nanoprobes as well their lack of cytotoxicity in macrophage populations RAW 264.7. Optical imaging in the mouse peritoneal region confirms the in vivo ability of one of the nanoprobes to localize inflammatory processes. In vivo imaging shows exosome uptake in the inflamed peritoneal region, and flow-cytometric analysis of peritonitis exudates confirms the uptake by macrophage and neutrophil populations. These results support the promising use of goat milk exosomes as natural probes in the detection of inflammatory processes.

1. Introduction

Extracellular vesicles (EVs) are signaling particles without replicative capacity, released by cells to the biological fluids with the aim of controlling intercellular communication.[1,2] Among these secreted particles, exosomes have been described as one of the smallest EVs (30–150 nm) and are of endosomal origin.[3] They carry and exchange proteins, lipids, miRNA, or DNA between diverse cell types.[1,4] These nanometric EVs have important roles in different biological processes, including tumor metastasis and tissue regeneration, and have been proposed as prognostic markers for different diseases.[5]

In light of their transport function, exosomes are currently under consideration as novel agents for diagnosis and therapy, especially as drug delivery systems (DDS). Traditionally, this application has been covered by various synthetic

A. Santos-Coquillat, M. I. González, M. González-Arjona, V. Albaladejo-García, M. Desco, B. Salinas
Unidad de Medicina y Cirugía Experimental
Instituto de Investigación Sanitaria Gregorio Marañón (IiSGM)
Madrid 28007, Spain
E-mail: mdesco@hggm.es; bsalinas@hggm.es

A. Santos-Coquillat, M. I. González, M. Desco, B. Salinas
Unidad de Imagen Avanzada
Centro Nacional de Investigaciones Cardiovasculares (CNIC)
Madrid 28029, Spain

A. Clemente-Moragón, B. Ibañez, E. Oliver
Myocardial Pathophysiology Area
Centro Nacional de Investigaciones Cardiovasculares Carlos III (CNIC)
Madrid 28029, Spain

The ORCID identification number(s) for the author(s) of this article can be found under https://doi.org/10.1002/smll.202105421.

DOI: 10.1002/smll.202105421

H. Peinado
Microenvironment and Metastasis Laboratory
Department of Molecular Oncology
Spanish National Cancer Research Center (CNIO)
Madrid 28029, Spain

J. Muñoz, P. Ximénez Embún
Proteomics Core Unit
ProteoRED-ISCIII
Spanish National Cancer Research Center (CNIO)
Madrid 28029, Spain

B. Ibañez, E. Oliver
CIBER de Enfermedades CardioVasculares (CIBERCV)
Madrid 28029, Spain

B. Ibañez
Cardiology Department
IIS-Fundación Jiménez Diaz University Hospital
Madrid 28015, Spain

M. Desco, B. Salinas
Centro de Investigación Biomédica en Red de Salud Mental (CIBERSAM)
Madrid 28029, Spain

M. Desco, B. Salinas
Departamento de Bioingeniería e Ingeniería Aeroespacial
Universidad Carlos III de Madrid
Madrid 28911, Spain

nanoparticles, principally liposomes.[6,7] Current barriers to the clinical use of biofunctionalized nanoparticles include lack of batch to batch reproducibility and toxicity. Naturally derived nanoparticles such as exosomes are increasingly being proposed as an alternative to synthetic nanoparticles to overcome some of those limitations, thanks to their natural origin, (phospho)lipid bilayer structure, and nanometric size.[8]

Among the possible sources, milk exosomes are notable for their easy production and high sample volumes in comparison with culture fluid or blood plasma. With this approximation, a high yield, harmless, and cost-effective production of non-tumor exosomes can be obtained for use as a scalable source.[9] In addition, the non-toxic and non-immunogenic behavior of milk exosomes in healthy models has been demonstrated,[10,11] as has as their application as carriers for chemotherapeutic/chemopreventive agents.[12] Although these characteristics have been evaluated in exosomes from different milk sources such as human, pig, rat, camel, and horse,[8] to the authors' knowledge goat milk exosomes have not yet been investigated.

Aside from the great potential of EVs in cancer therapy,[5,6] milk exosomes have been implicated in the regulation of inflammatory processes through miRNA trafficking.[13] Moreover, milk exosomes are rapidly trapped by macrophages[14,15] as part of the clearance activity that these cells, along with neutrophils, carry out when foreign agents are detected.[16–18] This natural targeting and their nanometric size support the use of milk exosomes in the diagnosis and therapy of inflammation underlying the pathogenesis of diseases such as atherosclerosis, chronic obstructive pulmonary disease, asthma, and cancer.[19,20]

The main aims of this work were a full physicochemical characterization of exosomes isolated from goat milk and their further evaluation for use as natural nanoprobes in the detection of inflammatory processes. This evaluation was performed through their fluorescent labeling and further in vitro and in vivo assessment by means of optical imaging. The internalization of these fluorescent exosomes in inflammatory M0, M1, and M2 macrophages in vitro was evaluated by means of confocal imaging and flow cytometry. Once the capacity of macrophages to internalize the exosomes was demonstrated in vitro, it was evaluated in vivo in a mouse peritonitis model in comparison with healthy mice by assessing the biodistribution of the probe through optical imaging. Finally, exudates from the peritonitis model were analyzed using flow cytometry and confocal imaging to confirm the in vivo uptake of the nanoparticles by specific inflammatory cell populations (macrophages and neutrophils).

2. Results and Discussion

2.1. Isolation and Characterization of Milk Exosomes

Our isolation protocol enabled us to collect pure goat's milk exosomes in suspension at 2.29 ± 0.25 mg mL^{-1}, as quantified by Coomassie-Bradford assay, from an initial goat's milk volume of 60 mL. Previous publications detailing exosome isolation techniques from culture media of dendritic and murine tumor cell lines have reported that only 0.2–2.0 µg of these nanovesicles per million cells could be isolated,[5,21,22] thus highlighting the potential of milk as an economic and scalable source of exosomes.

Transmission electron microscopy (TEM) images confirmed a non-aggregated population of exosomes with typical "cup-shape" morphology. Large extracellular vesicles (distinguishable by their irregular shape and electron-dense appearance,[8,23] cellular fragments, or protein clusters are often found in suspensions of isolated milk exosomes,[24] but these contaminants were not identified in the micrographs (**Figure 1**a). These results evidence the successful combination of ultracentrifugation, precipitation, and size exclusion chromatography for the isolation of goat milk exosomes. The protocol also removes other contaminants, such as milk fat.

Quantitative measurement of the hydrodynamic size by dynamic light scattering (DLS) established a mean size of 125.70 ± 3.25 nm (Figure 1b), with a polydispersity index of 0.14, confirming a monodisperse suspension of exosomes. Nanoparticle tracking analysis (NTA) showed modal average values of 124.44 ± 8.54 nm, similar to the results achieved by DLS. This size distribution matches the profile described for exosomes isolated from cow milk, one of the most employed sources for the collection of milk extracellular vesicles.[12,25] NTA also demonstrated the high content of nanovesicles in the exosome suspension, reporting a concentration of $3.32 \times 10^{11} \pm 3.25 \times 10^{11}$ particles mL^{-1} (Figure 1c).

2.2. Proteomic Evaluation of Milk Exosomes

To determine the composition of milk exosomes, extensive LC-MS/MS proteomic analyses were performed. A total of ≈900 proteins (derived from ≈4500 peptides) were identified in all three independent isolations of goat milk exosomal samples.

GO analyses using the top 100 most abundant proteins revealed enrichment in terms such as extracellular exosome, extracellular region part, vesicle, and membrane-bounded vesicle, confirming the identity of the samples as EVs (Figure S1, Supporting Information).

In addition, PANTHER overrepresentation analyses showed that the identified proteins were involved in processes such as neutrophil degranulation, the innate immune system, the immune system, hemostasis, and platelet activation. This kind of activity related to the immune system has been described for other milk-derived exosomes.[25] A 15-fold or greater enrichment was observed for the ECRT (endosomal sorting complex required for transport), endosomal/vacuole pathway, and regulation of the complement cascade, among others.

Similarly, proteins were involved in several molecular functions including membrane transport and binding activity, protein transport, vesicle-mediated transport, adhesion, or metabolic processes. These kinds of processes are related to general cell function and growth or to the endocytic pathway of the vesicles themselves. Other processes such as endosomal transport via the multivesicular body sorting pathway, that pathway itself, late endosome-to-vacuole transport, and response to reactive oxygen species were enriched more than tenfold. Cellular compartment results showed an over-representation of "endosome";

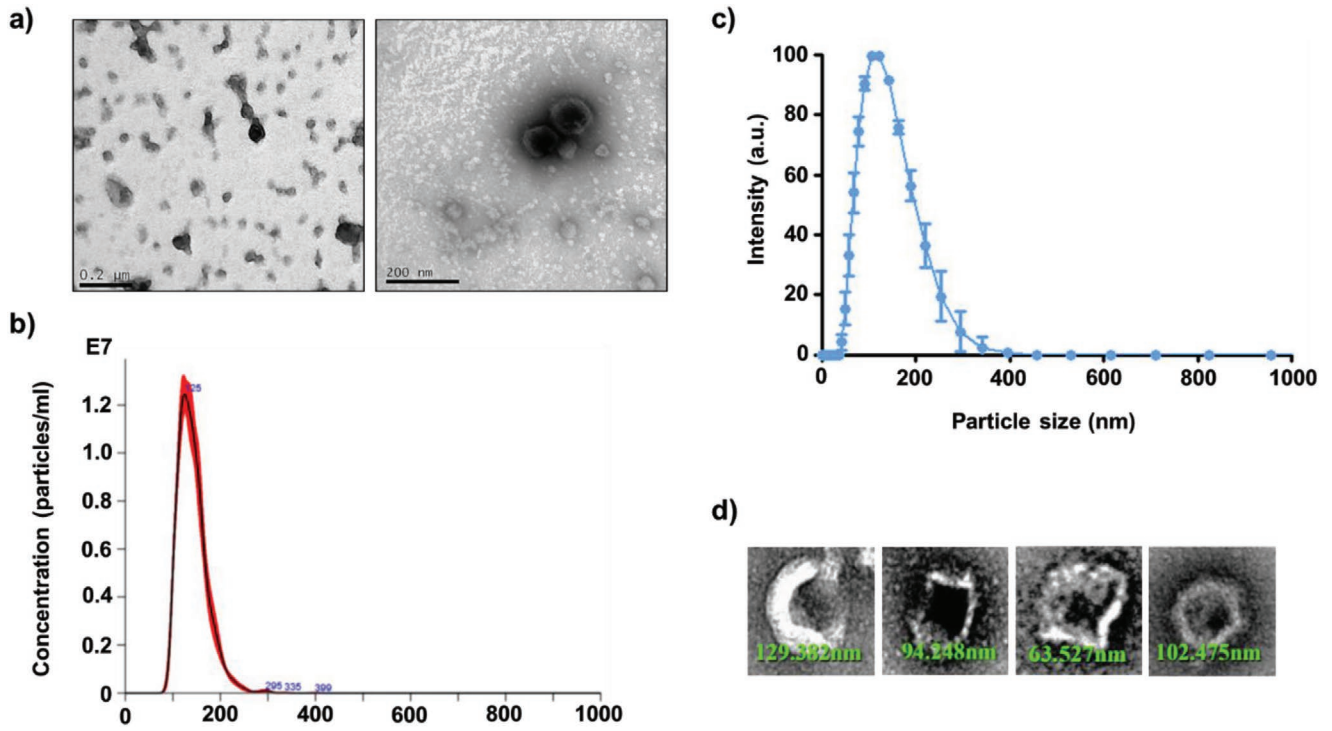

Figure 1. Physicochemical characterization of goat milk exosomes. a) Transmission electron microscopy images of isolated goat milk exosomes. b) Size distribution established by dynamic light scattering. c) Nanoparticle tracking analysis of goat milk exosomes. d) Electron microscopy of the nanovesicles.

this fact is of great importance, as exosomes differ from EVs in their cellular origin, which is the endocytic pathway.[26]

Among the identified proteins, butyrophilin, β-lactoglobulin, CD36, α-lactalbumin, albumin, and xanthine oxidoreductase were highly abundant, as they are in milk exosomes from cow, horse, and human.[8] To further confirm the exosomal nature of the nanoparticles, we compared our proteomic data with ExoCarta and found many of the main exosome markers. These include tetraspanins such as CD9, CD63, and CD81, and other classical markers like TSG101, HSP90AA1, HSP90AB1, and annexins. These markers define a unique composition that differs from other non-vesicular milk components and reveals the nanoparticles' exosomal nature.

2.3. Plasma Analysis of Healthy Mice Treated with Goat Milk Exosomes

Biochemical analysis of plasma did not show alterations in basic, hepatic, or inflammatory markers compared with those of control mice, thus ruling out any potential toxic effects associated with goat milk exosome administration (Table S1, Supporting Information and **Figure 2**).

Although previous publications confirmed the high accumulation of milk exosomes in liver after intravenous administration,[27,28] markers of hepatic damage, such as alanine aminotransferase and aspartate aminotransferase, did not differ between treated mice and controls (Figure 2).[29] The evaluation of blood markers related to the immune system and inflammatory activity, such as C-reactive protein, high and low-density lipoprotein (HDL and LDL), albumin, and cholesterol, also suggested that goat's milk exosomes did not significantly alter the inflammatory and immune profile of treated mice after 24 h (Figure 2). Only triglyceride values were reduced in treated mice compared with untreated mice (144.13 ± 52.43 mg dL^{-1} in treated mice and 228.14 ± 86.85 mg dL^{-1} in controls); this effect was previously described for bovine milk exosomes orally administered to rats.[12] These results confirm the in vivo biocompatibility and non-toxicity of goat milk exosomes. Nevertheless, this evidence is still insufficient to rule out the existence of mild or late immunogenic effects. Further research in this direction is warranted.

2.4. Fluorescence Labeling and Physicochemical Characterization of Exo-BDP and Exo-SCy5

In order to assess the behavior of goat milk exosomes in inflammatory processes, we used a chemical approach previously published by our group to fluorescently label the nanoparticles, creating two exosome-based optical probes.[28] The specific dyes employed in the labeling were selected based on the biological application: for in vitro assessment, the nanoparticles were labeled with the commercial fluorophore BODIPY-FL (Exo-BDP) as in our previous studies,[28] while for in vivo experiments, Sulfo-Cyanine 5 (Exo-SCy5) was selected for its favorable emission in the far red spectrum. The labeling success was demonstrated by fluorescence emission measurements using a fluorospectrometer, which registered over

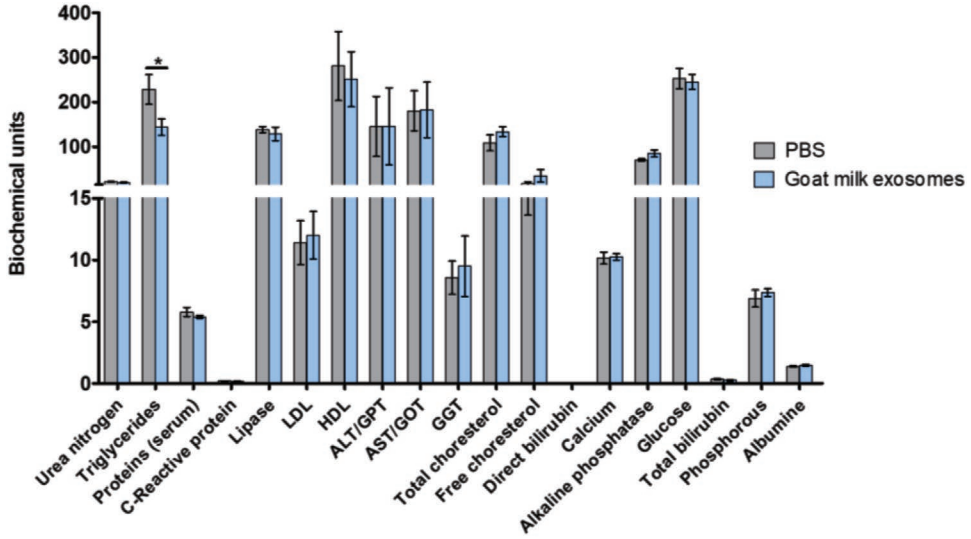

Figure 2. Biochemical profile of plasma samples from control (PBS) and treated (goat milk exosomes) mice, collected 24 h after dose administration. Asterisks (*) indicate statistically significant differences ($p < 0.05$), observed only for triglycerides.

4000 relative fluorescent units in both cases. Additionally, the fluorescence of the resulting probes was evaluated by flow cytometry (**Figure 3**), showing an intense peak between 10^5 and 10^6 for both Exo-BDP and Exo-SCy5. The whole analyzed population could be considered 100% positive for the labeling, as the control's autofluorescence of 10^1–10^3 relative fluorescent units did not overlap with that of the labeled exosomes in either wavelength.

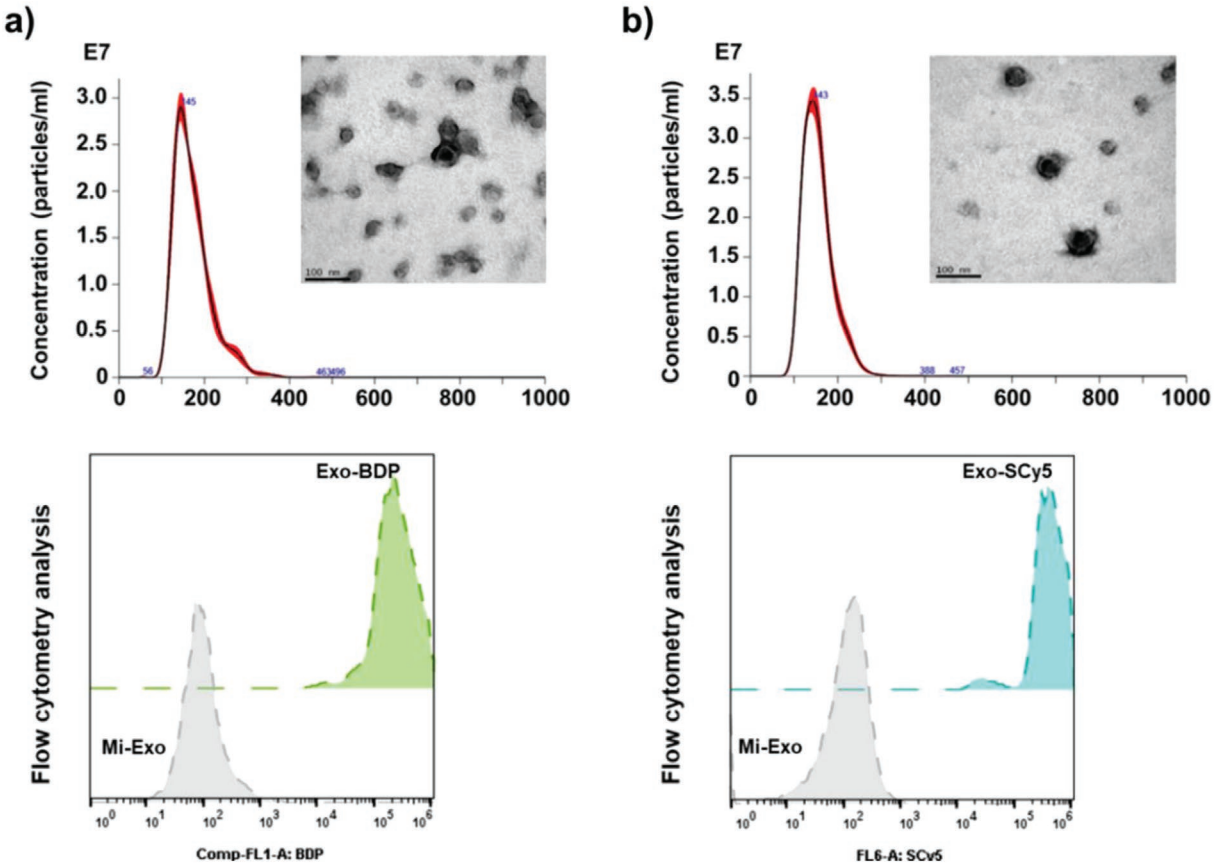

Figure 3. Physicochemical characterization of fluorescent milk exosomes, including NTA analysis, TEM images (100 000×), and flow cytometry for a) Exo-BDP and b) Exo-SCy5.

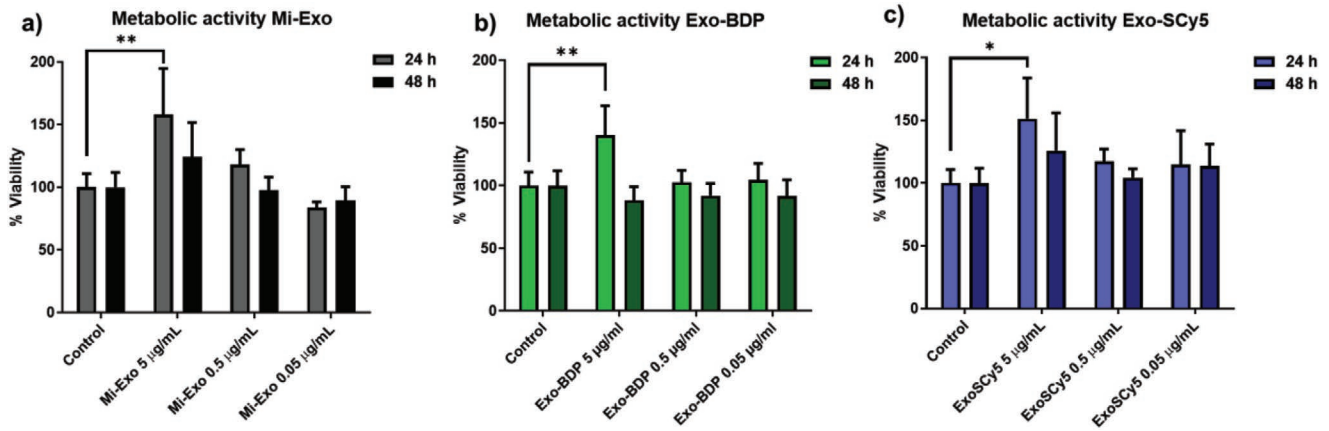

Figure 4. In vitro metabolic activity evaluation with RAW 264.7 cells. Metabolic activity levels by XTT assay after 24 and 48 h of dose of a) Mi-BDP, b) Exo-BDP, and c) Exo-SCy5 (5 μg/mL, 0.5 μg/mL, and 0.05 μg/mL). Statistical analysis by two-way ANOVA and Tukey's multiple comparisons test; P values below 0.05: * $p < 0.05$, ** $p < 0.01$.

The absence of morphological modifications after labeling was proven using TEM, showing that exosomes maintained their typical cup-shape appearance after the labeling reaction (Figure 3). Moreover, NTA eliminated the possibility of any significant alterations in the sizes of the exosomes, which measured 142.20 ± 2.80 nm (Exo-BDP) and 140.10 ± 3.80 nm (Exo-SCy5) (Figure 3). NTA also confirmed that the samples were highly enriched with exosomes after optical labeling and purification, showing values of $2.46 \times 10^{11} \pm 3.81 \times 10^{9}$ particles mL^{-1} for Exo-BDP and $2.72 \times 10^{11} \pm 4.00 \times 10^{9}$ particles mL^{-1} for Exo-SCy5. The slight reduction in the number of labeled particles compared with the control was acceptable, considering the loss of sample during purification.

2.5. Cytocompatibility Evaluation

XTT assay results (**Figure 4**a) showed that cells maintained their viability in the presence of different doses of Mi-Exo, Exo-SCy5, and Exo-BDP at 24 h and 48, despite the labeling of the nanoparticles. Nevertheless, at 24 h an increase in metabolic activity was found at the higher dose (5 μg mL^{-1}) of each nanoparticle type. This behavior has also been observed with other extracellular vesicles, for instance as a macrophage proliferation after 24 h and 48 of exposure.[30] A similar effect was previously found with other milk exosomes,[31–33] with cell metabolic activity increasing after exposure to the nanoparticles at different time points. This effect could be related to the fact that the macrophages are phagocytosing at 24 h and therefore, the metabolic activity increases at 24 h and decreases at 48 h, as most of the exosomes have already been internalized. An LDH assay was also performed with our novel nanoparticles (Figure S4, Supporting Information) to evaluate their cytotoxicity, based on the release of lactate dehydrogenase due to potential damage to the plasma membrane. These studies showed no significant differences 48 h after the addition of exosomes at various concentrations (5, 0.5, and 0.05 μg mL^{-1}), in accord with the results obtained with XTT.

2.6. In Vitro Uptake Studies Using Confocal Imaging of RAW 264.7 Cells

The evaluation of intracellular uptake of Exo-BDP at different concentrations (5, 0.5, and 0.05 μg mL^{-1}) by RAW 264.7 cells was assessed using confocal microscopy at 5 min, 1, 4, and 24 h (**Figure 5**). Figure 5a presents the confocal images 24 h after exosome addition at the three dosages. The 5 μg mL^{-1} dose induced the greatest incorporation of the exosomes into the cells, with almost all the cytoplasmic area positive for the Exo-BDP (green). This result can be correlated with the increase in metabolic activity observed at 24 h as measured with the XTT assay (Figure 4b). Figure 5b shows the uptake time course for the different concentrations of Exo-BDP (5, 0.5, and 0.05 μg mL^{-1}). All concentrations showed significant differences over time and between dosages ($p < 0.00001$ for both time and dosage).

2.7. In Vitro Assessment of Selective Uptake of Exo-BDP by M1, M2, and M0 Macrophages

Once we confirmed the uptake of the probe in macrophages, we evaluated the selectivity of the nanoprobe toward specific macrophage populations. Macrophage phenotypes (non-activated or activated) depend on their function and localization. Macrophages with these different phenotypes may incorporate the nanoprobe differently, showing different in vivo uptake. Activated macrophages (Mφ) are mainly classified as M1 (pro-inflammation) and M2 (anti-inflammation) macrophages.[34,35] M1 macrophages induce a type I immune response, killing microorganisms and tumor cells. M2 macrophages participate in a type II immune response by removing cellular debris residues and promoting angiogenesis.[36]

Using flow cytometry, we quantified Exo-BDP uptake in the different macrophage populations. To this purpose, we selected the intermediate concentration (0.5 μg mL^{-1}) of exosomes to better mimic the in vivo scenario. M0, M1, and M2 populations were evaluated after 1, 4, and 24 h of exposure to the exosomes (**Figure 6**a). The activated population with the proinflammatory

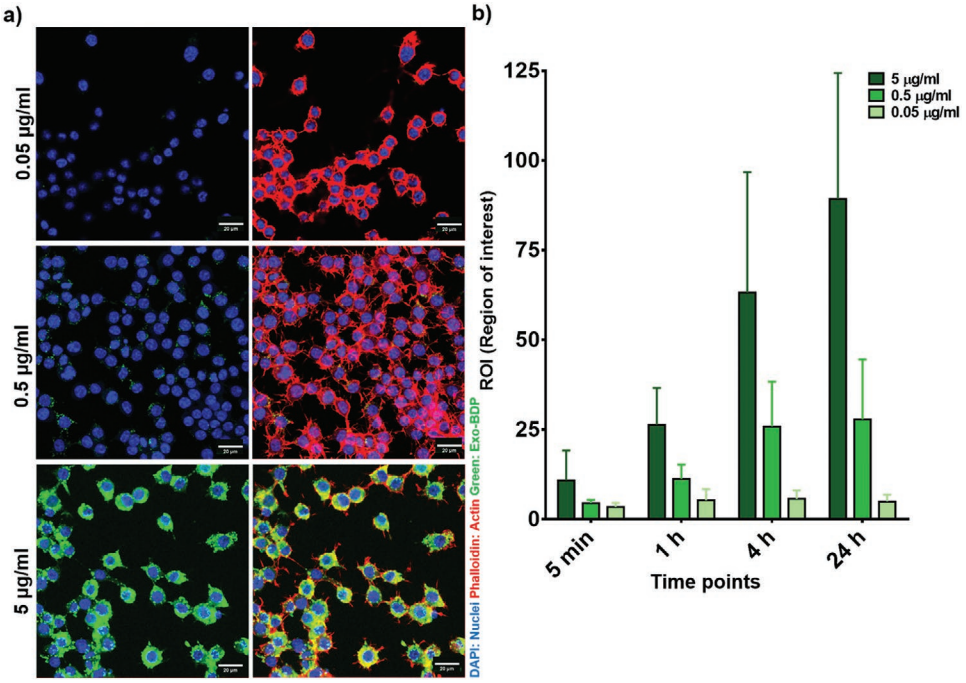

Figure 5. Assessment of exosome uptake by RAW 264.7 macrophages. a) Confocal images of macrophages after 24 h of exposure to different concentrations of exosomes. Blue (DAPI), red (phalloidin) and green (Exo-BDP). b) Quantification of fluorescent exosome uptake by RAW 264.7 cells in confocal imaging. Statistical analysis by ANOVA and post-hoc Student-Newman-Keuls multiple comparisons test.

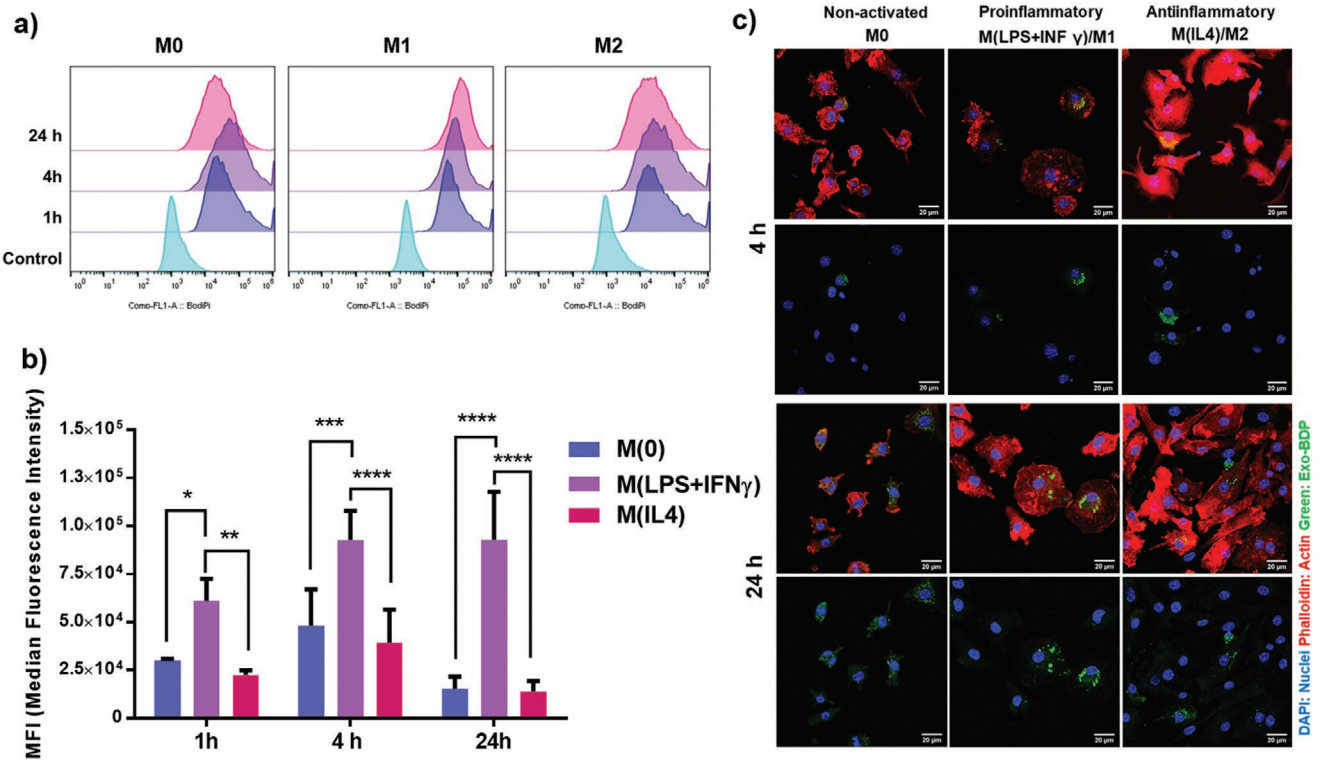

Figure 6. In vitro evaluation of Exo-BDP uptake in macrophage populations. a) Flow cytometry of M0, M1, and M2 populations after 1, 4, and 24 h of incubation with 0.5 µg mL^{-1} Exo-BDP. b) Quantification of fluorescence intensity by flow cytometry. Statistical analysis by two-way ANOVA and Tukey's multiple comparisons test; p values below 0.05: * $p < 0.05$, ** $p < 0.01$, *** $p < 0.001$, **** $p < 0.0001$. c) Confocal images of Exo-BDP uptake in M0, M(IFN-γ+LPS)/M1, and M(IL-4)/M2 populations. IFN-γ, interferon gamma; LPS, lipopolysaccharide; IL-4, interleukin-4.

stimuli (M1) presented higher uptake than the untreated cells (M0) and M2 (two-way ANOVA, $p < 0.01$). These differences were greater at 24 h, when the M1 population presented a fivefold increase in fluorescence compared with M0 and M2 (Figure 6b). This result was confirmed by confocal microscopy at the same time points (Figure 6c). At 1 h, Exo-BDP uptake did not differ among the macrophage populations, but from 4 h and up to 24 h there was a clear difference in the cytoplasmic disposition of the nanoparticles, with the proinflammatory phenotype M1 presenting tighter packing in contrast to a more diffuse distribution in the control M0 cells.

2.8. In Vivo Optical Imaging

Once we confirmed the in vitro capacity of inflammatory cells to incorporate the labeled exosomes, we carried out an in vivo assessment of our milk exosome-based probe to verify its ability to detect inflammatory processes. To this end we used a thioglycolate-induced mouse peritonitis model and chose the far-red exosome-based probe Exo-SCy5 to minimize interference by tissue autofluorescence. Based on previous studies with this animal model,[37–40] we selected 9 and 24 h time points (6 and 21 h after exosome administration) for image acquisition. In parallel, we carried out a similar imaging protocol employing healthy mice as a control group to evaluate the natural biodistribution of the probe.

In vivo optical imaging showed clear differences in the uptake of the nanoprobe between healthy mice and the thioglycolate-induced peritonitis model mice (**Figure 7**a). In the inflammation model, intense fluorescence was recorded 6 h post injection in the abdominal area, with progressive clearance up to 21 h after administration. This peritoneal accumulation associated with the inflammatory pathology was observed both in vivo and ex vivo. Control animals showed uptake of the nanoprobe mostly in the bladder and liver (Figure 7a and 7b) but not in the peritoneal area. The renal and hepatobiliary metabolism of the probe were observed in both the controls and the peritonitis model mice. Early uptake of intravenously injected exosomes in the liver has been reported and attributed to physiological phagocytosis of exosomes by macrophages.[27,41] In addition, an increase in the optical signal in the bladder due to the renal clearance of exosomes has also been described, with a progressive reduction of exosome accumulation in the liver as bladder activity increases.[42,43]

After the last time point of in vivo imaging, the mice were sacrificed, the skin of the abdominal area was removed, and the mice were imaged again. Figure 7b shows a higher signal in the liver and intestine of the peritonitis mice compared with the

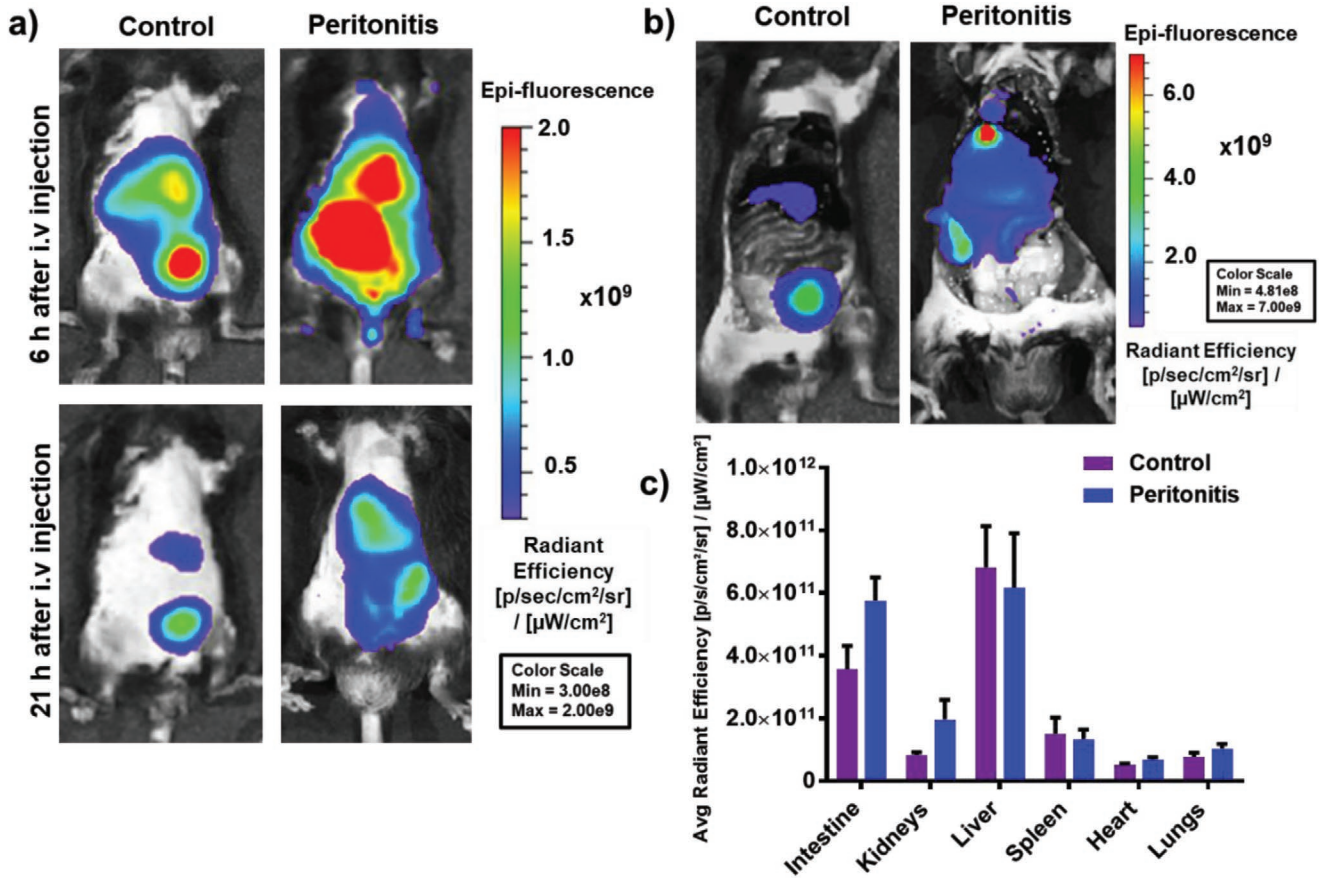

Figure 7. Abdominal in vivo uptake in a mouse peritonitis model. a) In vivo fluorescence imaging 6 and 21 h after Exo-SCy5 injection in a healthy mouse (control) and peritonitis model. b) Ex vivo fluorescence imaging after sacrifice and skin removal. c) Quantification of fluorescence signals of excised organs (intestine, kidneys, liver, spleen, heart, and lungs) from animals sacrificed 21 h after Exo-SCy5 injection.

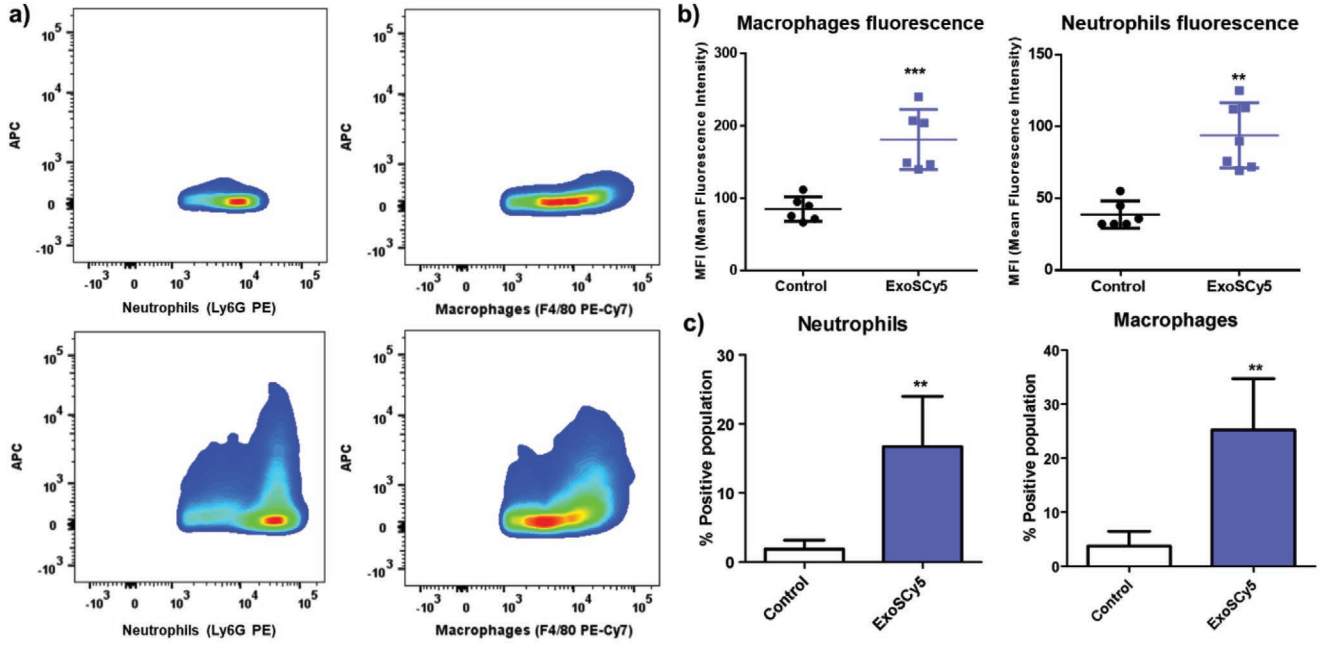

Figure 8. Flow cytometry of Exo-SCy5 in exudate neutrophils and macrophages. a) Representative dot plots of markers Ly6G in PE and F4/80 in PE-Cy7, respectively, versus exosome fluorescence (Cy5/APC). Untreated controls with peritonitis (upper) and treated with Exo-SCy5 (lower). b) MFI values of Exo-SCy5 uptake by neutrophils (left) and by macrophages (right), represented by median values from mice with peritonitis without Exo-SCy5 and treated with Exo-SCy5. c) Percentages of neutrophils and macrophages that have taken up fluorescent exosomes (Cy5/APC); control values stand for cell autofluorescence. p values below 0.05 indicate significant differences: * $p < 0.05$, ** $p < 0.01$, *** $p < 0.001$.

healthy controls, which mainly accumulated Exo-SCy5 in the bladder. Next, excised organs were imaged ex vivo (Figure S5, Supporting Information) and the signal was quantified (Figure 7c). In the peritonitis model we observed higher exosome content in the kidneys and intestines and lower fluorescence in liver and spleen compared with the controls, but not reaching statistically significant differences (Student's *t*-test) (Figure 7c).

2.9. Flow Cytometry of Peritonitis Exudates

To quantify the uptake of the Exo-SCy5 probe by the myeloid population (macrophages and neutrophils), we isolated peritoneal exudates from Exo-SCy5-treated and from untreated peritonitis model mice, which were used to assess cell autofluorescence. **Figure 8**a shows fluorescence intensity corresponding to exosomes (APC) for the neutrophil (Lys6G+) and macrophage (F4/80+) populations of the untreated control group (top) and the group treated with Exo-SCy5 (bottom). Probe intensity was quantified in terms of median fluorescence intensity (MFI) (Figure 8b). A statistically significant increase in MFI was observed in both cell populations with respect to the controls ($p = 0.0037$ and $p = 0.0006$ for macrophages and neutrophils, respectively). Exo-SCy5 was taken up by 27.8 ± 7.1% of the total macrophage population (Figure 8c) based on the fluorescence signal versus 3.7 ± 2.7% of the control due to their autofluorescence. In the case of neutrophils (Figure 8c) 18.4 ± 6.4% of the total population took up the probe, versus 1.8 ± 1.2% of the control population.

2.10. Confocal Imaging of Cells Sorted From Peritoneal Exudates

Finally, to visualize the uptake of our nanoprobe by the targeted cell population, we sorted positive SCy5 exudate samples. **Figure 9** presents a representative image of the final sorted pool. The incorporation of our nanoparticles can be observed in a neutrophil (stained for Ly6G) at the top of the image and in macrophages (stained for CD68) at the bottom of the figure. Similar to the in vitro results previously described (Figure 5), exosome fluorescence was observed in the perinuclear area, especially in neutrophils where the Exo-SCy5 seemed more localized in rounded packages.

3. Conclusion

In this work we present for first time goat milk exosomes as natural liposome-like nanoparticles and their use in the development of optical probes for the detection of inflammatory diseases. We present a complete physicochemical, biochemical and proteomic characterization of the novel nanoparticles that proved its exosomal and nanometric nature, as well as their non-toxicity in vivo. Supporting these data, XTT and LDH assays confirmed the excellent cytocompatibility of the exosomes. In vitro studies in RAW 264.7 macrophages showed a time and dose dependent uptake, and a higher uptake of the M1 proinflammatory activated population compared to M(0) and M2. In addition, successful in vivo internalization of the fluorescent nanoparticles by macrophages and/or neutrophils was demonstrated in a peritonitis mouse model. All these findings suggest that goat milk exosomes are able to localize

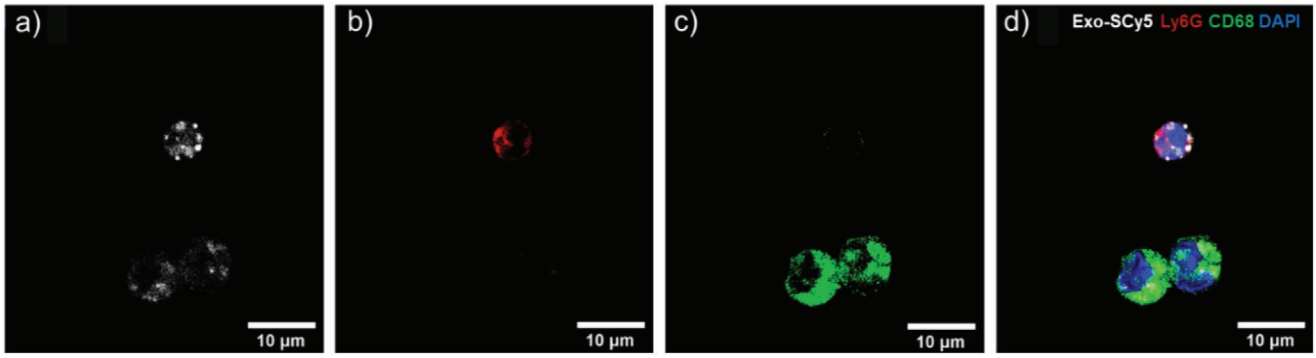

Figure 9. Confocal imaging of cells obtained from FACS and immunostained with specific antibodies. a) The Exo-SCy5 signal is white. b) Neutrophils stained for Ly6G are red. c) Macrophages stained for CD68 are green. d) Four-channel merged image. Cellular nuclei were stained with DAPI (blue).

inflammatory processes and support its potential use as markers for the in vivo detection of inflammatory processes by optical imaging.

4. Experimental Section

Isolation of Milk Exosomes: Exosomes were isolated by differential centrifugation and ultracentrifugation, complemented with size exclusion chromatography. All steps of the isolation protocol were carried out at 4 °C in an AVANTI J-30I centrifuge (Beckman Coulter Instruments, CA, USA), fitted out with a Ja 30,50 Ti fixed-angle rotor (k factor = 280) and 30-ml polycarbonate tubes, as already described in the literature.[27,28]

Commercial pasteurized semi-skimmed goat's milk (El Cantero de Letur, Spain) was centrifuged at 5000 G for 10 min to remove fat globules (MFGs). Microbial rennet was then added to improve the precipitation of casein. Resultant milk whey was centrifuged at 5000 and 13 000 G for 10 and 35 min respectively, then 15 min at 35 000 G and finally 70 min at 100 000 G. This process allows the precipitating of exosomes excluding large extracellular vesicles and cell debris. The exosomal pellet was washed thrice with phosphate-buffered saline (1X PBS) and then purified with PD-10 columns (GE Healthcare Bio-Sciences AB, IL, USA). Exosomes were re-isolated at 100 000 G for 90 min and the resultant pellet was dispersed in 100–200 µL of 1X PBS. Exosomes suspension was stored at –20 °C until used.

Total protein content was estimated by Coomassie-Bradford colorimetric assay employing a microplate-reader (680 XR, BIO-RAD Laboratories, CA, USA).

Physicochemical Characterization: Transmission electron microscopy (TEM): Morphological characteristics of exosomes were assessed using a JEOL JEM-1010 from ICTS Centro Nacional de Microscopía Electrónica (Universidad Complutense de Madrid, Spain), which operates at 100 kV. Formvar carbon coated copper grids were employed for the negative staining of exosomes with uranyl acetate at room temperature. Samples were previously filtered through 0.45 µm.

Dynamic Light Scattering (DLS): Size distribution of exosomes was established employing a Zetasizer Nano (Malvern Panalytical, UK), equipped with DTS0012 disposable cuvettes (Brand, Germany). Measurements were performed in triplicate, selecting protein as the sample material and water as dispersant.

Nanoparticle Tracking Analysis (NTA): Real-time concentration (particles mL^{-1}) of exosomes was quantified using a NanoSight NS500 (NanoSight, UK), fitted out with a sCMOS camera. Specific temperature was not selected for the recording and samples were filtered through 0.45 µm and infused under controlled and constant flow. Camera level and threshold were established at 11 and 25, respectively. Five consecutive 60 s videos were recorded per sample and analyzed by NTA 3.4 Build software. Replicated histograms were averaged for the modal size distribution assessment.

Proteomic Study of Milk Exosomes: Sample preparation for proteomic analysis: The protein content of goat's milk exosomes was solubilized using 8 M urea in 100 mM Tris-HCl (pH 8.0). Samples (20 µg) were digested using the standard FASP protocol. Briefly, proteins were simultaneously reduced (15 mM TCEP) and alkylated (30 mM CAA) for 30 min in the dark at room temperature, and sequentially digested with Lys-C (protein:enzyme ratio 1:50, overnight at room temperature; Wako) and with trypsin (protein:enzyme ratio 1:100, 6 h at 37 °C; Promega, WI, USA). Resulting peptides were desalted using C18 stage-tips.

Mass spectrometry: For the proteomic analysis of goat milk-derived exosomes we used liquid chromatography with tandem mass spectrometry (LC-MS/MS) by coupling an Ultimate 3000 RSLCnano System (Dionex) with a Q-Exactive Plus mass spectrometer (Thermo Fisher Scientific, CA, USA). Peptides were loaded into a trap column (Acclaim PepMapTM 100, 100 µm × 2 cm, Thermo Fisher Scientific, CA, USA) over 3 min at a flow rate of 10 µL min^{-1} in 0.1% FA. Then peptides were transferred to an analytical column (PepMapTM RSLC C18, 2 µm, 75 µm × 50 cm, Thermo Fisher Scientific, CA, USA) and separated using a 90 min effective linear gradient (buffer A: 0.1% FA; buffer B: 100% ACN, 0.1% FA) at a flow rate of 250 nL min^{-1}. The gradient used was: 0–5 min 4% B, 5–7 min 6% B 7–60 min 17.5% B, 60–72.5 min 21.5% B, 72.5-80 min 25% B, 80–94 min 42.5% B, 94–100 min 98% B, 100–110 min 4% B. The peptides were electrosprayed (2.1 kV) into the mass spectrometer through a heated capillary at 320 °C and a S-Lens RF level of 50%. The mass spectrometer was operated in a data-dependent mode, with an automatic switch between the MS and MS/MS scans using a top 15 method (minimum AGC target 3E3) and a dynamic exclusion time of 26 s. MS (350–1500 m/z) and MS/MS spectra were acquired with a resolution of 70000 and 17500 FWHM (200 m/z), respectively. Peptides were isolated using a 2 Th window and fragmented using higher-energy collisional dissociation (HCD) at 27% normalized collision energy. The ion target values were 3E6 for MS (25 ms maximum injection time) and 1E5 for MS/MS (45 ms maximum injection time). Samples were analyzed twice.

Proteomic data analysis: Raw files were processed with MaxQuant (v 1.6.1.0) using the standard settings against a Bovidae protein database (UniProtKB/Swiss-Prot/TrEMBL October 2018, 92, 108 sequences) supplemented with contaminants. Label-free quantification was done with match between runs (match window of 0.7 min and alignment window of 20 min). Carbamidomethylation of cysteines was set as a fixed modification whereas methionine oxidation and N-term acetylation were variable protein modifications. The minimal peptide length was set to 7 amino acids and a maximum of two tryptic missed-cleavages were allowed. The results were filtered at 0.01 FDR (peptide and protein level) and subsequently the "proteinGroup.txt" file was loaded in Perseus (v1.6.0.7) for further analysis. Statistical overrepresentation of GO Terms, Reactome and Panther pathways were performed using Panther v15.0. The Bos taurus database was considered as the reference list and a Fisher's Exact test with FDR correction (5%) was applied.

The MS proteomic data have been deposited to the ProteomeXchange Consortium via the PRIDE partner repository with the dataset identifier PXD025026. For peer reviewing purposes, the data set can be accessible under the username reviewer_pxd025026@ebi.ac.uk and password: W8uD0thG.

Biochemical Assessment of Milk Exosomes in Plasma of Healthy Mice: Possible toxic effects of goat milk exosomes were evaluated in vivo on CD1 mice (13 weeks old; Charles River Laboratories International Inc., MA, USA) employing the same concentrations as in the in vivo imaging studies. Animals were randomized into two groups, control ($n = 7$) and treated ($n = 8$), which were intravenously injected through the lateral tail vein with either PBS (100 µL) or goat milk exosomes (20 µg, 100 µL in PBS), respectively. Blood samples were collected 24 h post-injection by cardiac puncture and plasma was separated from whole blood by centrifuging 5 min at 84 000 rpm.

Complete biochemical analysis of blood plasma was carried out by Comparative Medicine Department of Centro Nacional de Investigaciones Cardiovasculares (CNIC) Carlos III (Spain), including basic, hepatic and inflammatory profiles.

Fluorescence Labeling of Exosomes: Goat milk exosomes were labeled with BODIPY-FL NHS ester (BDP) or Sulfo-Cyanine 5 (SCy-5) (Lumiprobe, Germany), following previously described protocols.[28] Suspension of 100 µg of milk exosomes in 100 µL of 1X PBS was adjusted to pH 8.5 using a 0.1 M $NaHCO_3$ solution. Then, exosomes were mixed with 10 µL of BDP-FL (12.5 mM) or SCy-5 (17 mK) and vortex for 2 h at 4 °C. Free fluorophore residues were removed by purification with Exosome Spin Columns (Invitrogen, CA, USA).

Fluorescence Labeling Characterization: Flow cytometry: Flow cytometry analysis was performed using a Gallios ten color Flow Cytometer (Beckman Coulter Instruments, CA, USA). Exo-BDP suspensions were excited employing a blue light laser (Excitation: 488 nm; detection FL1 Emission: 525/20nm) and a red light laser (Excitation: 633 nm detection FL6 Emission: 660/20nm) was used for the excitation of Exo-SCy5 suspensions. Data were analyzed using FlowJo (Ashland, OR, USA) software.

Fluorescence emission assessment: The fluorescence spectra of Exo-BDP and Exo-SCy5 were recorded using a NanoDrop 3300 fluorospectrometer (Thermo Fisher Scientific, CA, USA), measuring Exo-BDP with the Blue LED with λ excitation = 515 nm and Exo-SCy5 with the White LED with λ excitation = 665 nm.

Cell Culture: RAW 264.7 (ATCC TIB-71) murine cell line was used as a model of inflammatory response mediated by macrophages. For maintenance of the cell line the medium was changed every other day and cells were cultured in Dulbecco's MEM (D6429, Sigma Aldrich, MO, USA) with 10% Fetal Bovine Serum (FBS, gibco, 10 270) and 1% penicillin, streptomycin and amphotericin B (17-745H, Lonza, Switzerland) incubated at 37 °C with 5% CO2. Subculturing was performed with a cell scraper (3011, Corning Costar, NY, USA).

XTT Assay: Metabolic activity of macrophages was measured at 24 and 48 h using CyQUANT TM XTT assay (Invitrogen, Thermo Fisher Scientific, CA, USA), a non-toxic technique that quantitatively measures the cellular redox potential, providing an estimation of viability. 1.5×10^4 cells were seeded on a 48-well plate (Corning Costar, NY, USA) and 5, 0.5, and 0.05 µg mL^{-1} dose of exosomes were added (Mi-Exo, Exo-BDP, Exo-SCy5). Each well received 140 µL of XTT dye, and the plates were incubated for 180 min at 37 °C. Absorbance of each well was measured using a plate-reader (680 XR, BIO-RAD Laboratories, CA, USA) at 450 nm. Each condition was analyzed in triplicate.

LDH Assay: LDH Cytotoxicity assay kit (Pierce, Thermo Fisher Scientific, CA, USA) is a colorimetric method that quantifies cellular cytotoxicity based on the plasma membrane damage. RAW 264.7 were seeded on 96-well plates at a concentration of 1.5×10^4 cells and evaluated after 48 h of Mi-Exo, Exo-BDP or Exo-SCy5 incubation (5, 0.5, and 0.05 µg mL^{-1}). Briefly, 10 µL of sterile ultrapure water or lysis buffer were added to control conditions, corresponding to spontaneous release or maximum LDH release, and cultured for 45 min in an incubator at 37 °C with 5% CO_2. After this time, 50 µL of each condition/sample medium was transferred to a 96-well plate and mixed with 50 µL of Reaction Mixture. The new plate was incubated at RT for 30 min in darkness and finally, 50 µL of Stop Solution was added to each sample. Absorbance of each well was measured using a plate-reader (680 XR, BIO-RAD Laboratories, CA, USA) at 450/655 nm.

In Vitro Fluorescence Uptake: RAW 264.7 cells were plated on 24-well plates with glass coverslips at 1.5×10^4 cells cm^{-2} in complete DMEM. 5, 0.5, and 0.05 µg mL^{-1} dose of Exo-BDP were added to evaluate the uptake level after 5 min, 1, 4, and 24 h. Cells growing on the glass coverslips were fixed with 3.7% formaldehyde solution for 10 min after the exosomes uptake. After formaldehyde was removed, cells were washed three times with PBS and stained with Phalloidin-iFluor 555 Reagent (ab176756, Abcam, UK) for actin and DAPI staining (D9542, Sigma Aldrich, MO, USA) for nuclei during 20 min at RT (Room Temperature) and in darkness. Dako Fluorescence Mounting Medium (Agilent, CA, USA) was used to prepare the coverslips for microscopy and left to cure overnight. Cells were observed using a confocal microscope (Leica-SPE, Leica Microsystems, Germany) at 488 nm (Exo-BDP), 555 nm (Phalloidin) and 405 nm (DAPI). ROI (region of interest) of the fluorescent images was calculated using ImageJ software taking an average 50 cells per condition.

Macrophages Activation: Macrophages were activated with 30 ng mL^{-1} IL-4 (Peprotech, UK) for M(IL-4) and 20 ng mL^{-1} of IFN-γ (Peprotech, UK) and 100 ng mL^{-1} LPS (Sigma Aldrich, MO, USA) for M(IFN-γ+LPS). M(IL-4) population was identify as M2 and M(IFN-γ+LPS) as M1. RAW 264.7 cells were seeded on 24-well plates with glass coverslips or 12-well plates at 1.5×10^4 cells per cm^2 in complete DMEM for confocal microscopy or flow cytometry, respectively. After 24 h of stimuli, 0.5 µg mL^{-1} of Exo-BDP were added to be evaluated by confocal microscopy and flow cytometry.

In Vitro Flow Cytometry: For flow cytometry RAW 264.7 cells were seeded at a concentration of 2×10^6 cells cm^{-2} in 12-well plates. Cells were detached with trypsin/EDTA (T3924, Sigma Aldrich, MO, USA) and washed twice with PBS after each centrifugation. Propidium iodide (P4864, Sigma Aldrich, MO, USA) was used in order to evaluate the cell viability after the stimuli and Exo-BDP uptake. A Gallios flow cytometer was used and analyzed with the Flowjo (Ashland, OR, USA) software.

In Vivo and Ex Vivo Fluorescence Imaging: All animal experiments were carried out in accordance with the EU Directive (2010/63EU) and Recommendation 2007/526/EC, enacted in Spanish law under Real Decreto 53/2013. Animal protocols were approved by the local ethics committees and the Animal Protection Area of the Comunidad Autónoma de Madrid.

In vivo assessment of the selectivity of the nanoparticle towards inflammatory processes was assessed using a well-established mouse model of thioglycolate-induced peritonitis.[44,45] Briefly, 8–13-week-old wild-type C57BL/6 mice ($n = 6$) were intraperitoneally injected with 1 mL of thioglycolate (BD211716). Three hours after the thioglycolate injection, the animals received an intravenous (i.v.) administration of Exo-SCy5 (100 µL in PBS, 20 µg) through the tail vein. As control group for the evaluation of the natural biodistribution of the nanoparticles, healthy animals ($n = 6$) were also injected with the nanoparticles, employing same imaging protocol. In vivo fluorescence image acquisition was performed with an IVIS Spectrum 200 In vivo Imaging System (Perkin Elmer, MA, USA) 6 and 21 h after exosome injection, both in peritonitis and control mice, using a Cy5.5 filter, Em = Cy5.5, Ex = Cy5.5. During image acquisition mice were kept anesthetized with 2.5% isofluorane in 100% of O_2 via facemask. Analysis and quantification of the images was performed with Living Image 4.4 Software (Perkin Elmer).

After the last time point of the image acquisition (24 h post injection of thioglycolate and 21 h post Exo-SCy5 administration) animals were sacrificed, a peritoneal lavage was carried out and organs of interest (intestine, liver, spleen, heart, and lungs) were harvested to perform ex vivo assessment by fluorescence imaging. Fluorescence was quantified as average radiant efficiency, expressed as mean ± SD, in $(p\ s^{-1}\ cm^{-2}\ sr^{-1})/(\mu W\ cm^{-2})$.

Flow Cytometry of Exudates: Exosome uptake by myeloid cells (macrophages and neutrophils) was assessed by flow cytometry after in vivo imaging acquisition. Exudates were obtained from

thioglycolate-induced peritonitis mice (n = 6), after the latest imaging time-point (21 h). For the evaluation of autofluorescence of inflammatory cells, we also included a control group with peritonitis but without nanoparticles administration (n = 6). For exudate collection, animals were sacrificed and peritoneal lavage performed with 2 mL of saline (NaCl, 0.9%). Samples were gently centrifuged (200 g, 5 min) and washed with 1X PBS. Cells were then incubated for 30 min with a rat PE-conjugated anti-mouse Ly6G (Clone: 1A8, 551 461, BD Pharmingen, CA, USA) antibody or a rat PE-Cy7-conjugated anti-mouse F4/80 antigen pan-macrophage marker (Clone: BM8, 123 114, BioLegend, CA, USA) antibody. After the incubation, cell nuclei were stained with DAPI (D8417, Sigma Aldrich, MO, USA). All samples were filtered using 100 µm Cell Strainer (352 360, Falcon) before the analysis for exactly 60 s of constant medium flow in a FACS Canto-3L flow cytometer equipped with DIVA software (BD Biosciences, NJ, USA). All experiments were conducted at the CNIC-Cellomics Unit.

Exosome Uptake Analyses: Flow cytometry was used to evaluate the uptake of fluorescent exosomes into myeloid cells isolated from peritoneal exudates. The entire cell sample was labeled with DAPI and dead cells (positive labeling for DAPI) were excluded from the analysis. Within the live cell population, macrophage and neutrophil populations were selected using F4/80 and Ly6G markers, respectively. On the identified populations we measured the median fluorescence intensity (MFI) in the FL6 channel (APC), corresponding to Exo-SCy5. In addition, the percentage of the population positive for probe incorporation was determined in both cell lines. All results were analyzed using FlowJo software (Ashland, OR, USA).

Cell Sorting and Immunofluorescence: To confirm and visualize the internalization of the Exo-SCy5 probe by confocal microscopy, the cell populations present in the peritoneal exudates were isolated by sorting, at the wavelength of the probe (630 nm), using an Aria Cell Sorter at the CNIC-Cellomics Unit.

Once sorted, cells were gently centrifuged (200 G, 5 min) and fixed in 2% paraformaldehyde. After fixation, cells were washed with 1X PBS and placed onto Superfrost Plus slides (Thermo Fisher Scientific, CA, USA), until samples were dehydrated and cells stuck to the slide. Then, cells were blocked in 1X PBS and 3% normal goat's serum, and then incubated overnight at 4 °C with a rat anti-mouse CD68 (Clone: FA-11, MCA1957, BIO-RAD Laboratories, CA, USA) antibody. After that, cells were incubated for 1 h with an anti-rat Alexa Fluor-488 conjugated-secondary antibody. After washing thrice with 1X PBS, they were incubated overnight at 4 °C with a rat PE-conjugated anti-mouse Ly6G antibody, counterstained with DAPI to visualize the nuclei and covered with Fluoroshield (F6182, Sigma Aldrich, MO, USA). Images were then acquired with a Leica SP8 Confocal Navigator Microscope available at CNIC's Microscopy Unit.

Statistics: All data are represented as mean ± standard deviation (SD). Comparisons between PBS group and Mi-Exo treated group were performed with Student's t tests. XTT statistical analysis was performed using two-way ANOVA and Tuckey's multiple comparison test. LDH statistical analysis was performed using one-way ANOVA and Tuckey's multiple comparison. Statistical analysis of macrophages uptake employing different concentrations and timepoints in confocal imaging was performed by two-way ANOVA and post-hoc Student-Newman-Keuls multiple comparisons test. Analysis of the fluorescence intensity of the macrophages populations was performed using two-way ANOVA and Tuckey's multiple comparison test. For in vivo and ex vivo peritonitis data a KS Normality test was used to determine if variables followed a normal distribution. Comparisons between control and Exo-SCy5 groups were performed by Student's t test. All data were analyzed using Prism software 8.4.3 (Graph pad, Inc.) except confocal macrophages uptake, performed with SPSS. Differences were considered statistically significant for p values below 0.05.

Supporting Information

Supporting Information is available from the Wiley Online Library or from the author.

Acknowledgements

This study has been funded by Instituto de Salud Carlos III, through the project "PI20/01632", co-funded by European Regional Development Fund (ERDF), "A way to make Europe" and by Comunidad de Madrid, project "Y2018/NMT-4949 (NanoLiver-CM)" and "S2017/BMD-3867 (RENIM-CM)", co-funded by European Structural and Investment Fund. This work has been also supported by "Diagnosis and treatment follow-up of severe Staphylococcal Infections with Anti-Staphylococcal antibodies and Immune-PET - Grant Fundación BBVA a Equipos de Investigación Científica 2018". A. Santos-Coquillat is grateful for financial support to Consejería de Educación e Investigación, co-financed by European Social Fund (ESF) grant PEJD-2018-POST/BMD-9592. A. Santos Coquillat is also funded by Instituto de Salud Carlos III, co-funded by European Social Fund "Investing in your future" (grant CD19/00136). The CNIC is supported by the Instituto de Salud Carlos III (ISCIII), the Ministerio de Ciencia e Innovación (MCIN) and the Pro CNIC Foundation. The CNIO Proteomics Unit is funded by the H2020 project EPIC-XS (ref. 823839). Biomedical Imaging has been conducted at the Advanced Imaging Unit of the CNIC (Centro Nacional de Investigaciones Cardiovasculares Carlos III), Madrid, Spain. The authors thank Izaskun Bilbao and Iria Sánchez Lobo for their excellent work with animal preparation, and Gorka Sobrino for the assistance in exosomes isolation. The authors also thank Marta García Camacho, from the Comparative Medicine Department, for her support with the biochemical analysis. Microscopy was conducted at the Microscopy & Dynamic Imaging Unit, CNIC, Madrid, Spain, supported by FEDER, "Una manera de hacer Europa" and Confocal Unit from Unidad de Medicina y Cirugía Experimental of Hospital Universitario Gregorio Marañón, Madrid, Spain. Flow cytometry was conducted at the Celomics Unit CNIC, Madrid, Spain, and Flow Cytometry Unit from Unidad de Medicina y Cirugía Experimental of Hospital Universitario Gregorio Marañón, Madrid, Spain. Cell culture was conducted in Cell Culture Unit from Unidad de Medicina y Cirugía Experimental of the Hospital Universitario Gregorio Marañón, Madrid, Spain.

Conflict of Interest

The authors declare no conflict of interest.

Author Contributions

A.S.-C. and M.I.G. contributed equally to this work. The manuscript was written through contributions of all authors. All authors have given approval to the final version of the manuscript.

Data Availability Statement

The MS proteomic data have been deposited to the ProteomeXchange Consortium via the PRIDE partner repository with the dataset identifier PXD025026. For peer reviewing purposes, the data set can be accessible under the username reviewer_pxd025026@ebi.ac.uk and password: W8uD0thG.

Keywords

exosomes, fluorescence imaging, goat milk, inflammation, macrophages, nanoparticles, peritonitis

Received: September 6, 2021
Revised: October 29, 2021
Published online: December 2, 2021

[1] S. Mathivanan, H. Ji, R. J. Simpson, *J. Proteomics* **2010**, *73*, 1907.
[2] C. Thery, K. W. Witwer, E. Aikawa, M. J. Alcaraz, J. D. Anderson, R. Andriantsitohaina, A. Antoniou, T. Arab, F. Archer, G. K. Atkin-Smith, D. C. Ayre, J. M. Bach, D. Bachurski, H. Baharvand, L. Balaj, S. Baldacchino, N. N. Bauer, A. A. Baxter, *J. Extracell. Vesicles* **2018**, *7*, 1535750.
[3] E. R. Abels, X. O. Breakefield, *Cell. Mol. Neurobiol.* **2016**, *36*, 301.
[4] J. P. Armstrong, M. N. Holme, M. M. Stevens, *ACS Nano* **2017**, *11*, 69.
[5] H. Peinado, M. Aleckovic, S. Lavotshkin, I. Matei, B. Costa-Silva, G. Moreno-Bueno, M. Hergueta-Redondo, C. Williams, G. Garcia-Santos, C. Ghajar, A. Nitadori-Hoshino, C. Hoffman, K. Badal, B. A. Garcia, M. K. Callahan, J. Yuan, V. R. Martins, J. Skog, R. N. Kaplan, M. S. Brady, J. D. Wolchok, P. B. Chapman, Y. Kang, J. Bromberg, D. Lyden, *Nat. Med.* **2012**, *18*, 883.
[6] X. Li, A. L. Corbett, E. Taatizadeh, N. Tasnim, J. P. Little, C. Garnis, M. Daugaard, E. Guns, M. Hoorfar, I. T. S. Li, *APL Bioeng.* **2019**, *3*, 011503.
[7] F. Man, P. J. Gawne, R. T. M. de Rosales, *Adv. Drug Delivery Rev.* **2019**, *143*, 134.
[8] S. E. Sedykh, E. E. Burkova, L. V. Purvinsh, D. A. Klemeshova, E. I. Ryabchikova, G. A. Nevinsky, Milk Exosomes: Isolation, Biochemistry, Morphology, and Perspectives of Use, IntechOpen **2019**, https://www.intechopen.com/chapters/67488.
[9] S. Sedykh, A. Kuleshova, G. Nevinsky, *Int. J. Mol. Sci.* **2020**, *21*, 6646.
[10] O. P. B. Wiklander, J. Z. Nordin, A. O'Loughlin, Y. Gustafsson, G. Corso, I. Mäger, P. Vader, Y. Lee, H. Sork, Y. Seow, N. Heldring, L. Alvarez-Erviti, C. I. E. Smith, K. Le Blanc, P. Macchiarini, P. Jungebluth, M. J. A. Wood, S. E. L. Andaloussi, *J. Extracell. Vesicles* **2015**, *4*, 26316.
[11] X. Zhu, M. Badawi, S. Pomeroy, D. S. Sutaria, Z. Xie, A. Baek, J. Jiang, O. A. Elgamal, X. Mo, K. Perle, J. Chalmers, T. D. Schmittgen, M. A. Phelps, *J. Extracell. Vesicles* **2017**, *6*, 1324730.
[12] R. Munagala, F. Aqil, J. Jeyabalan, R. C. Gupta, *Cancer Lett.* **2016**, *371*, 48.
[13] J. D. Galley, G. E. Besner, *Nutrients* 745, **2020**, *12*.
[14] H. Izumi, M. Tsuda, Y. Sato, N. Kosaka, T. Ochiya, H. Iwamoto, K. Namba, Y. Takeda, *J. Dairy Sci.* **2015**, *98*, 2920.
[15] C. Lässer, V. S. Alikhani, K. Ekström, M. Eldh, P. T. Paredes, A. Bossios, M. Sjöstrand, S. Gabrielsson, J. Lötvall, H. Valadi, *J. Transl. Med.* **2011**, *9*, 9.
[16] H. H. Gustafson, D. Holt-Casper, D. W. Grainger, H. Ghandehari, *Nano Today* **2015**, *10*, 487.
[17] M. H. Lin, C. F. Lin, S. C. Yang, C. F. Hung, J. Y. Fang, *J. Biomed. Nanotechnol.* **2018**, *14*, 66.
[18] S. Manca, B. Upadhyaya, E. Mutai, A. T. Desaulniers, R. A. Cederberg, B. R. White, J. Zempleni, *Sci. Rep.* **2018**, *8*, 11321.
[19] Y. Kim, H. Mok, *Appl. Biol. Chem.* **2019**, *62*, 26.
[20] D. Okin, R. Medzhitov, *Curr. Biol.* **2012**, *22*, R733.
[21] E. Segura, C. Nicco, B. r. r. Lombard, P. Véron, G. a. Raposo, F. d. r. Batteux, S. Amigorena, C. Théry, *Blood* **2005**, *106*, 216.
[22] C. Théry, S. Amigorena, G. Raposo, A. Clayton, *Curr. Protoc. Cell Biol.* **2006**, *30*, 3.22.1.
[23] C. Thery, M. Ostrowski, E. Segura, *Nat. Rev. Immunol.* **2009**, *9*, 581.
[24] M. Kotmakçı, G. Erel Akbaba, *Exosome Isolation: Is There an Optimal Method with Regard to Diagnosis or Treatment?*, IntechOpen, London **2017**, pp. 163–182.
[25] M. Samuel, D. Chisanga, M. Liem, S. Keerthikumar, S. Anand, C.-S. Ang, C. G. Adda, E. Versteegen, M. Jois, S. Mathivanan, *Sci. Rep.* **2017**, *7*, 5933.
[26] J. Kowal, M. Tkach, C. Théry, *Curr. Opin. Cell Biol.* **2014**, *29*, 116.
[27] M. I. Gonzalez, P. Martin-Duque, M. Desco, B. Salinas, *Nanomaterials* **2020**, *10*, 1062.
[28] M. I. G.-A., M. González, A. Santos-Coquillat, J. Vaquero, E. Vázquez-Ogando, A. de Molina, H. Peinado, M. Desco, B. Salinas, *Biomedicines* **2021**, *9*, 81.
[29] F. W. Quimby, R. H. Luong, in *The Mouse in Biomedical Research*, (Eds: Fox, J. G. , Davisson, M. T. , Quimby, F. W. , Barthold, S. W. , Newcomer, C. E. , Smith, A. L.), 2nd ed., Academic Press, Burlington, **2007**, pp. 171–216.
[30] L. Cao, H. Xu, G. Wang, M. Liu, D. Tian, Z. Yuan, *Int. Immunopharmacol.* **2019**, *72*, 264.
[31] T. Chen, M.-Y. Xie, J.-J. Sun, R.-S. Ye, X. Cheng, R.-P. Sun, L.-M. Wei, M. Li, D.-L. Lin, Q.-Y. Jiang, Q.-Y. Xi, Y.-L. Zhang, *Sci. Rep.* **2016**, *6*, 33862.
[32] A. Hock, H. Miyake, B. Li, C. Lee, L. Ermini, Y. Koike, Y. Chen, P. Määttänen, A. Zani, A. Pierro, *J. Pediatr. Surg.* **2017**, *52*, 755.
[33] L. Wang, Z. Shi, X. Wang, S. Mu, X. Xu, L. Shen, P. Li, *Eur. J. Nutr.* **2020**, *60*, 317.
[34] M. Genin, F. Clement, A. Fattaccioli, M. Raes, C. Michiels, *BMC Cancer* **2015**, *15*, 577.
[35] S.-J. Park, B. Kim, S. Choi, S. Balasubramaniam, S.-C. Lee, J. Y. Lee, H. S. Kim, J.-Y. Kim, J.-J. Kim, Y.-A. Lee, N.-Y. Kang, J.-S. Kim, Y.-T. Chang, *Nat. Commun.* **2019**, *10*, 1111.
[36] A. Shapouri-Moghaddam, S. Mohammadian, H. Vazini, M. Taghadosi, S.-A. Esmaeili, F. Mardani, B. Seifi, A. Mohammadi, J. T. Afshari, A. Sahebkar, *J. Cell. Physiol.* **2018**, *233*, 6425.
[37] J. Chan, P. J. Leenen, I. Bertoncello, S. I. Nishikawa, J. A. Hamilton, *Blood* **1998**, *92*, 1423.
[38] A. D. Cook, E. L. Braine, J. A. Hamilton, *J. Immunol.* **2003**, *171*, 4816.
[39] U. Fiedler, Y. Reiss, M. Scharpfenecker, V. Grunow, S. Koidl, G. Thurston, N. W. Gale, M. Witzenrath, S. Rosseau, N. Suttorp, A. Sobke, M. Herrmann, K. T. Preissner, P. Vajkoczy, H. G. Augustin, *Nat. Med.* **2006**, *12*, 235.
[40] P. C. Leijh, T. L. van Zwet, M. N. ter Kuile, R. van Furth, *Infect. Immun.* **1984**, *46*, 448.
[41] D. H. Kim, V. K. Kothandan, H. W. Kim, K. S. Kim, J. Y. Kim, H. J. Cho, Y. K. Lee, D. E. Lee, S. R. Hwang, *Pharmaceutics* **2019**, *11*, 649.
[42] F. Royo, U. Cossío, A. Ruiz de Angulo, J. Llop, J. M. Falcon-Perez, *Nanoscale* **2019**, *11*, 1531.
[43] A. Banerjee, V. Alves, T. Rondão, J. Sereno, Â. Neves, M. Lino, A. Ribeiro, A. J. Abrunhosa, L. S. Ferreira, *Nanoscale* **2019**, *11*, 13243.
[44] A. Clemente-Moragón, M. Gómez, R. Villena-Gutiérrez, D. V. Lalama, J. García-Prieto, F. Martínez, F. Sánchez-Cabo, V. Fuster, E. Oliver, B. Ibáñez, *Eur. Heart J.* **2020**, *41*, 4425.
[45] J. Garcia-Prieto, R. Villena-Gutierrez, M. Gomez, E. Bernardo, A. Pun-Garcia, I. Garcia-Lunar, G. Crainiciuc, R. Fernandez-Jimenez, V. Sreeramkumar, R. Bourio-Martinez, J. M. Garcia-Ruiz, A. S. Del Valle, D. Sanz-Rosa, G. Pizarro, A. Fernandez-Ortiz, A. Hidalgo, V. Fuster, B. Ibanez, *Nat. Commun.* **2017**, *8*, 14780.